

Non-flux purification behavior of AZ91 magnesium alloy

WU Guo-hua(吴国华)^{1,2}, DAI Ji-chun(戴吉春)^{1,2}, SUN Ming(孙明)^{1,2}, DING Wen-jiang(丁文江)^{1,2}

1. National Engineering Research Center of Light Alloy Net Forming,
Shanghai Jiao Tong University, Shanghai 200240, China;

2. State Key Laboratory of Metal Matrix Composites, Shanghai Jiao Tong University, Shanghai 200240, China

Received 23 October 2009; accepted 1 July 2010

Abstract: The effects of non-flux purification techniques on the mechanical properties and microstructure of AZ91 magnesium alloy were investigated by ICP, OM, XRD and SEM. The results show that Ar spraying with high flow rate could remove non-metallic inclusions and improve the mechanical properties of AZ91. The alloy obtains the best properties after argon spraying for 30 min at the melt temperature of 740 °C. The ceramic foam filter (CFF) could effectively improve the ultimate tensile strength and elongation of AZ91 alloy, especially the elongation, which increase with increasing pores per inch (ppi) and the thickness of CFF. Non-flux purification does not change the microstructure of AZ91 alloy. However, filtration has a certain effect on the fracture pattern of AZ91 alloy. To improve the mechanical properties effectively, both filtration and gas spraying should be utilized together.

Key words: AZ91 magnesium alloy; inclusions; non-flux purification; argon spraying; ceramic foam filter; filtration

1 Introduction

Magnesium alloys have been proved to be highly competitive materials for construction purposes and automotive applications, especially when weight is a critical parameter[1–3]. However, the non-metallic inclusions in magnesium alloys such as MgO and Mg₃N₂ destroy the continuity of the magnesium matrix, and thus impair the mechanical properties of the alloys[4–5]. Refining technologies can be divided into two categories: flux-based technology and non-flux technology. The former method of refining magnesium scrap is relatively old but most common. However, the introduction of flux to the magnesium melt increases the chance of adding additional impurities. Sometimes large flux inclusions get trapped in the magnesium, causing deterioration of certain physical properties. Therefore, flux-based refining techniques are not the ultimate solution for magnesium refining[6]. Non-flux recycling based on gas spraying, melt filtration and settling, etc is a relatively new method to purify magnesium alloys[7].

At present, no research on the effects of gas bubbling incorporating ceramic foam filter (CFF) purification on the microstructure and mechanical

properties of AZ91 are reported. The purpose of this research is to investigate the effects of gas bubbling incorporating CFF purification on the microstructure and mechanical properties of AZ91 alloys.

2 Experimental

The chemical compositions of AZ91 alloy used in this experiment were measured by an inductively coupled plasma spectrum machine (ICP), as shown in Table 1. Tools and raw stuff used in the experiment were heated to 200 °C in stove before the experiment in order to eliminate the water remaining in them. 6 kg Mg alloy stuff was melted in a 2.5 kW crucible electric resistance furnace at one time, and a thermocouple was immersed in the melt directly to control the melt temperature by a temperature-control instrument. The liquid metal surface was protected from oxidation by using 0.5% (volume fraction) SF₆ in CO₂.

Table 1 Chemical compositions of AZ91 alloy (mass fraction, %)

Al	Zn	Mn	Be	Fe	Cu	Si	Ni	Mg
9.05	0.715	0.29	0.0011	0.0021	0.006	0.030	<0.001	Bal.

Foundation item: Project(08XD14020) supported by the Program of Shanghai Subject Chief Scientist, China; Project(2007CB613701) supported by the National Basic Research Program of China; Project(2009AA033501) supported by the National High-tech Research and Development Program of China

Corresponding author: WU Guo-hua; Tel: +86-21-54742630; Fax: +86-21-34202794; E-mail: ghwu@sjtu.edu.cn
DOI: 10.1016/S1003-6326(09)60414-3

During melting, a rotary impeller made of steel was inserted into the melt and inert gas, Ar, was injected through the impeller. The gas bubbling system was shown in Fig.1. The hole size in the rotary impeller head was 0.2 mm in diameter. The rotating speed was 120 r/min. The gas was dispersed into fine bubble clouds by the impeller and the bubbles attached to the oxides during their rising to the surface of the melt. Finally, the oxides raised to the surface of the melt and then were skimmed. The spraying spans varied from 20 to 60 min, the flow rates were 0–2 L/min and the metal temperature was 700–760 °C.

After purification, the melt was poured into five metallic moulds and moulded at pouring and mould temperatures of (720 ± 3) °C and (200 ± 10) °C, respectively. Fig.2 shows the photos of casting mould.

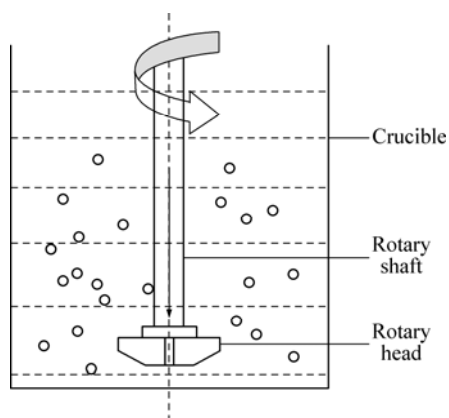


Fig.1 Schematic drawing of rotating impeller degassing system

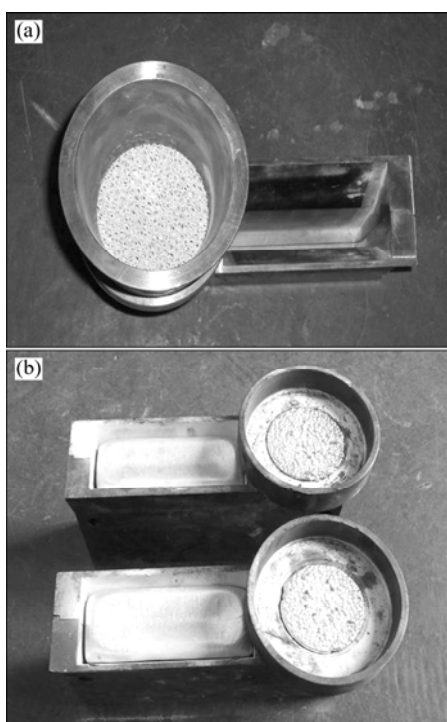


Fig.2 Photos of experimental casting mould: (a) Before casting; (b) After casting

The permanent moulds were coated with boron nitride. The mould was removed from the stove and pouring started once the preparations were completed. Fig.3(a) shows the photos of castings. CFFs were placed over the sprue of the permanent moulds. The CFFs used in these experiments are shown in Fig.3(b), they mainly consist of 70% Al_2O_3 , 15% SiO_2 and 10% ZrO_2 (mass fraction). The filter material was tested with respect to its reactivity with magnesium melt. The elements in the filter did not dissolve noticeably in the melt. Filter manufacturers commonly characterized the pore size of the filters by the number of pores per linear inch (ppi). Filters with pore sizes of 10, 15 and 20 ppi were used, and the approximate pore sizes were thus 2.5, 1.87 and 1.25 mm, respectively.

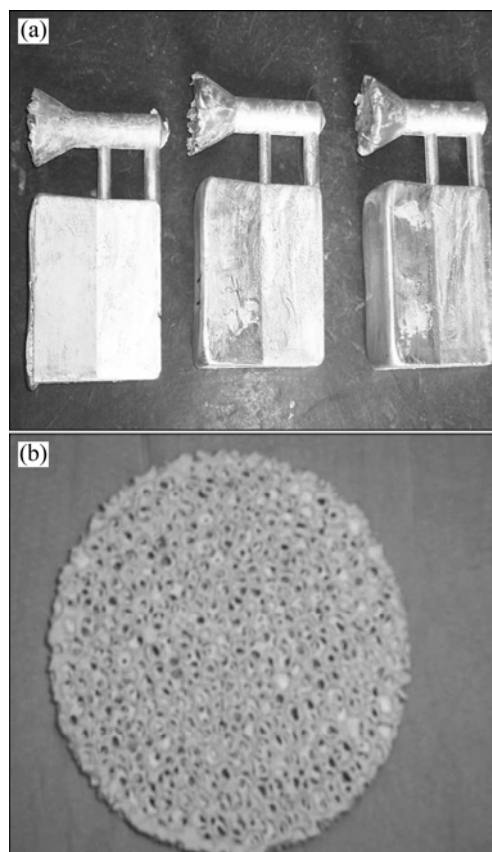


Fig.3 Photos of castings (a) and Al_2O_3 CFF (b)

The castings were cut to obtain tensile samples. The tensile specimens were tested using an Instron Series IX automated testing machine according to ASTM B557M specification. The gage length, width and thickness of the samples are 25, 6 and 3 mm, respectively. The yield strength (σ_s) at 0.2% offset, ultimate tensile strength (σ_b) and elongation (δ) were determined for each test bar. All the tests were carried out at a strain rate of 1.5 mm/min. Three specimens under the same condition were tested and the final values of the test were obtained in term of their average values. A Rigaku Dmax-rc X-ray

diffractometer(XRD) and a scanning electron microscope (SEM) JSM-5800 were employed to analyze the phase composition and morphology of fractures, respectively. Detailed microstructure investigations were completed.

3 Results

3.1 Effects of gas bubbling on mechanical properties

Fig.4 shows the effects of gas bubbling parameters on the mechanical properties. The effects of Ar flow rate on the mechanical properties are shown in Fig.4(a), in which the gas bubbling span is 30 min and the melt temperature is 730 °C during gas bubbling process. It can be seen surprisingly that the σ_b and σ_s of the gas bubbling sample at 0.5 L/min flow rate are lower than those of the sample from the fresh melt. When the Ar flow rate is 0.5 L/min, σ_b and σ_s decrease from 175.3 and 110.3 MPa to 168.8 and 96 MPa, respectively. However, when the flow rate increases to 2.0 L/min, σ_b and σ_s increase to 180.6 and 110.5 MPa, respectively. It can also be seen from Fig.4(a) that δ increases with increasing flow rate indicating that high flow rate is helpful to improve the mechanical properties. This means that Ar spraying with high flow rate can remove non-metallic inclusions from the melt. In fact, gas spraying also helps to degas the metal[8]. The process of Ar spraying to the melt eliminates any signs of gross amounts of dissolved gas.

Fig.4(b) shows the effects of Ar spraying time on the mechanical properties while the Ar flow rate is 2.0 L/min and the melt temperature is 730 °C. It can be seen that after Ar spraying for 30 min, σ_b and δ increase from 175.3 MPa and 2.74% to 180.6 MPa and 3.53%, respectively. This means that this process provides a certain refining action in which the non-metallic inclusions and dissolved gas may be floated to the top of the melt and subsequently non-metallic inclusions skimmed off. However, σ_b and δ will somewhat decrease with further increase of spraying time. Fig.4(b) also shows that long spraying time is detrimental to σ_s .

While the spraying time is 30 min and flow rate is 2 L/min, the effects of melt temperature during Ar spraying process on the mechanical properties are shown in Fig.4(c). It indicates that 740 °C helps to get the highest σ_b and δ values of 183.9 MPa and 3.54%, respectively. However, σ_b and δ decrease with further increase of melt temperature during spraying. This may result from the inclusion content under high treatment temperature.

3.2 Effects of CFF filtration on mechanical properties

Figs.5(a)–(b) show the effects of the filter porosity and thickness on the mechanical properties, respectively. It can be seen in Fig.5(a) that the CFF is 20 mm in thickness, σ_b and δ increase with increasing ppi, especially δ . CFF of 20 ppi increases σ_b and δ from

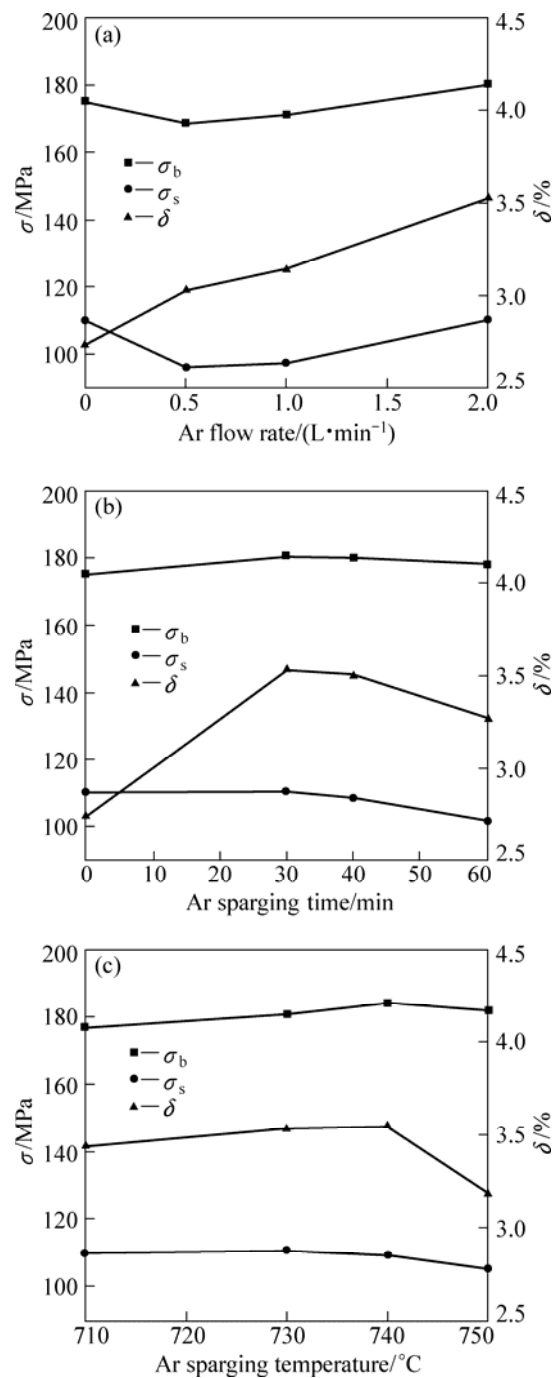


Fig.4 Effects of gas flow rate (a), spraying time (b) and spraying temperature (c) on mechanical properties of AZ91 magnesium alloy

175.3 MPa and 2.74% to 189.1 MPa and 4.02% by 7.9% and 46.7%, respectively. This means that δ can be greatly improved by filtration. It can also be seen from Fig.5(a) that the filter has no dramatic effect on σ_s . HOUSH and PETROVICH[8] reported that the use of filter significantly reduced the amount of large inclusions remaining in the melt, and an effective way was to reduce the hole size to trap smaller inclusions. From Fig.5(a), it can be concluded that σ_b and δ can be

improved with the decrease of inclusions in the melt. However, the inclusion content might have little effect on σ_s . Furthermore, in our experiments, it is found that the CFFs of more than 20 ppi tend to choke the metal flow. Hence, considering the success of filtration process, the CFF of 20 ppi is suitable for filtrating the melt.

Fig.5(b), in which the CFF is of 20 ppi, shows the effects of the thickness of CFF on the mechanical properties. It indicates that the use of CFF of 10 mm in thickness increases σ_b and δ from 175.3 MPa and 2.74% to 185.6 MPa and 3.72% by 5.9% and 35.8%, respectively. As the thickness increases from 10 to 20

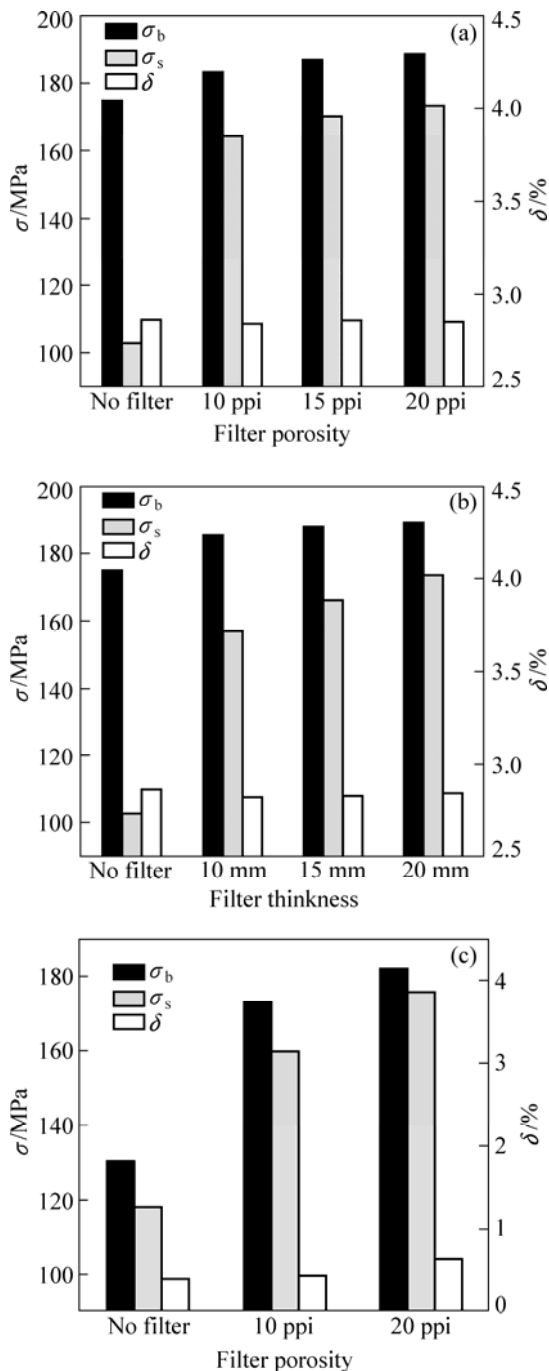


Fig.5 Effects of ppi of CFF (a), thickness of CFF (b) and filtration (c) on mechanical properties of AZ91 scraps

mm, σ_b and δ increase from 185.6 MPa and 3.72% to 189.3 MPa and 4.02% by 2% and 8%, respectively. It can also be seen from Fig.9 that the thickness of CFF has no dramatic effect on σ_s .

Fig.5(c) shows the effects of filtration on the mechanical properties of AZ91 scraps. The scraps consist of casting runner, riser head and waste casting, etc. It is seen that the CFF is 20 mm in thickness and very effective to increase the σ_b and δ of AZ91 scraps. The use of CFF of 10 ppi increases σ_b and δ from 130.4 MPa and 1.26% to 173.0 MPa and 3.15% by 32.7% and 150.0%, respectively, and the use of CFF of 20 ppi increases σ_b and δ from 130.4 MPa and 1.26% to 182.0 MPa and 3.86% by 39.6% and 206.3%, respectively. This means the σ_b and δ of AZ91 scraps can be improved greatly by filtration. Additionally, it still can be seen from Fig.5(c) that filtration has no dramatic effect on σ_s . Therefore, it can be concluded that inclusions have great effect on σ_b and δ , but little effect on σ_s .

3.3 Effects of gas bubbling incorporating filtration on mechanical properties

Figs.6(a)–(c) show the effects of gas bubbling incorporating filtration on the mechanical properties of AZ91 virgin metal. Fig.6 shows the effect of the ppi of CFF on the mechanical properties, in which Ar spraying flow at 2 L/min for 30 min at the melt temperature of 730 °C is performed before filtered by CFF of 20 mm in thickness. It is clear from this figure that σ_b and δ increase with the increase of ppi. After filtered by CFF of 20 ppi, σ_b and δ improve from 180.6 MPa and 3.53% to 192.1 MPa and 4.22% by 6.4% and 19.5%, respectively. However, σ_s does not change obviously.

Fig.6(b) describes the effects of CFF thickness on the mechanical properties with the gas bubbling incorporating filtration process, in which Ar spraying flow at 2 L/min for 30 min at melt temperature of 730 °C is performed before filtered by CFF of 20 ppi. It can be seen that σ_b and δ increase with the increase of filter thickness, especially δ . Compared with no filtration, σ_b and δ purified by CFF of 10 mm in thickness increase from 180.6 MPa and 3.53% to 189.7 MPa and 3.99% by 5.0% and 13.0%, respectively. However, when the thickness of CFF increases from 10 to 20 mm, σ_b and δ only increase from 189.7 MPa and 3.99% to 192.1 MPa and 4.22% by 1.3% and 5.7%, respectively. So it can be concluded that the thickness of CFF only has small effect on the mechanical properties.

Fig.6(c) describes the effects of gas flow rate on the mechanical properties during gas bubbling incorporating filtration process, in which Ar spraying flow for 30 min at melt temperature of 730 °C is performed before filtered by CFF of 20 ppi. It can be seen that at the initial Ar flow rate of 0.5 L/min, σ_b and σ_s decrease from

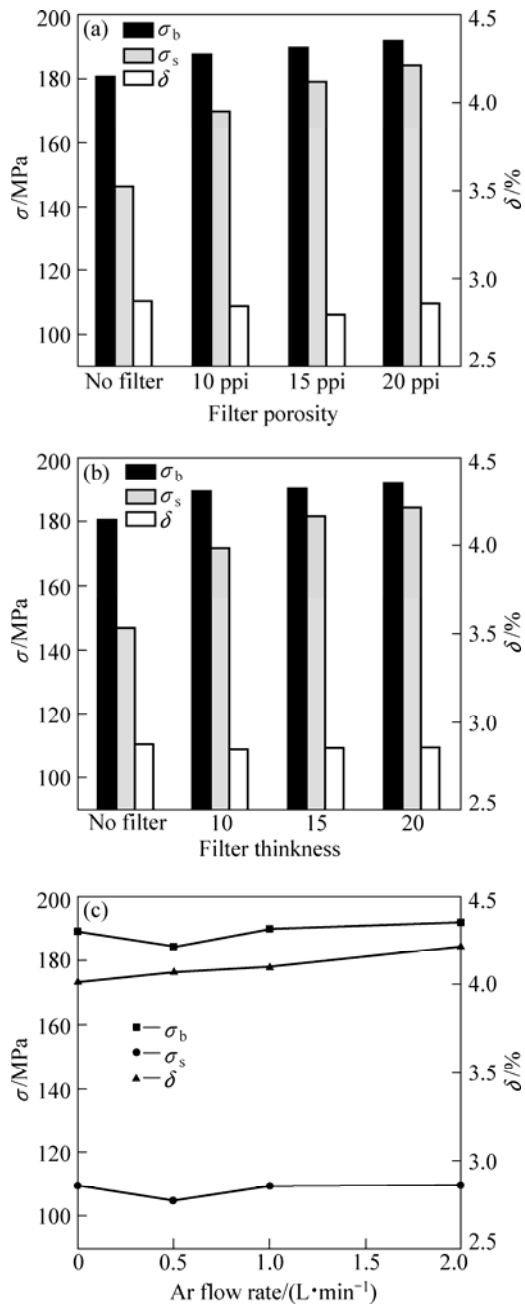


Fig.6 Effects of ppi (a), thickness of CFF incorporating gas bubbling (b) and gas flow rate incorporating filtration (c) on mechanical properties of AZ91 magnesium alloy

189.3 MPa and 109.3 MPa to 184.4 MPa and 104.7 MPa, respectively. However, when the flow rate increases to 2.0 L/min, σ_b and σ_s increase to 192.1 and 109.6 MPa, respectively. And from Fig.6(c), it can be seen that δ increases with the increase of flow rate. Fig.6(c) also indicates that the large flow rate is helpful to improve the mechanical properties.

3.4 Effects of non-flux purification on microstructure and fracture morphology

The microstructures of the unrefined AZ91

magnesium alloys are shown in Fig.7. The white matrix phase is α -Mg, the gray phase along the grain boundary is β -Mg₁₇Al₁₂ and the black particles are non-metallic inclusions. This figure shows that many inclusions exist in the unrefined magnesium alloys. Figs.7(a)–(c) show the inclusion clusters, dispersoids and film morphologies, respectively. Significantly larger inclusion clusters and dispersoids are present in the melt and few inclusion films are also noted. It should be pointed out that these photomicrographs provide information regarding the inclusion type, size, and morphology in unrefined AZ91 alloy. Individual inclusions such as MgO particles are about 10–30 μ m in size, while clusters of these inclusions range from 50–500 μ m in size, film oxides such as MgO extend to 200–400 μ m in length. This

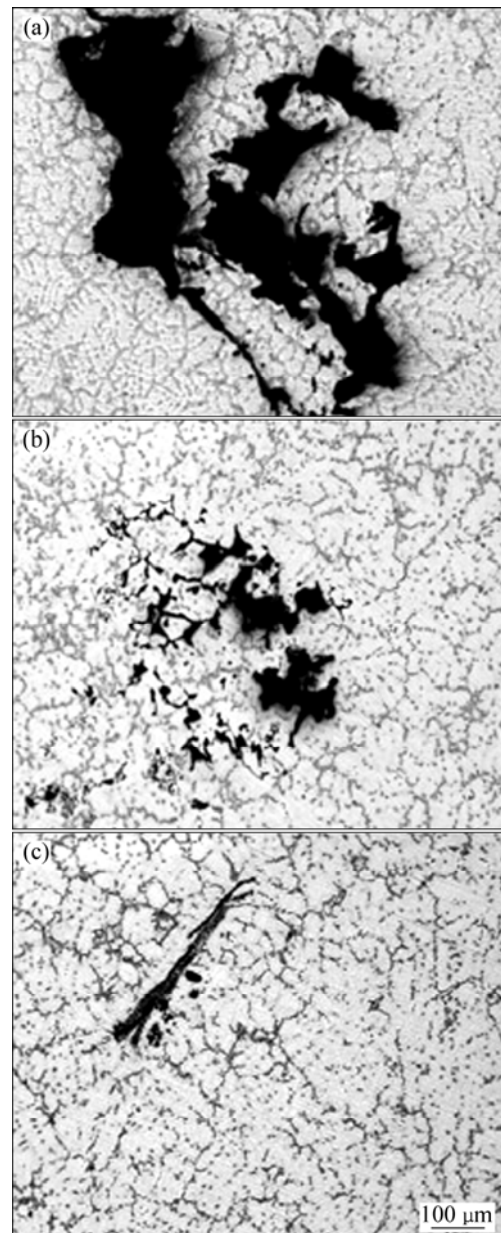


Fig.7 SEM images of cluster-like (a), dispersoid-like (b) and film-like (c) inclusion in unrefined AZ91 alloys

entails that substantial efforts should be paid to remove these inclusions. Fig.8(a) shows the microstructure of the sample purified by gas bubbling, in which the treatment time is 30 min under 730 °C at flow rate of 2 L/min. It can be seen that the large inclusion agglomeration can be dispersed by gas spraying. The microstructure of the specimen purified by the combination of CFF and gas bubbling is shown in Fig.8(b). It is clear that the inclusions are reduced substantially and clean melt can be achieved. The XRD analysis in Fig.9 shows that the alloy still consists of primary α -Mg and β -Mg₁₇Al₁₂, indicating that gas bubbling or filtration do not change the microstructure of AZ91 alloy.

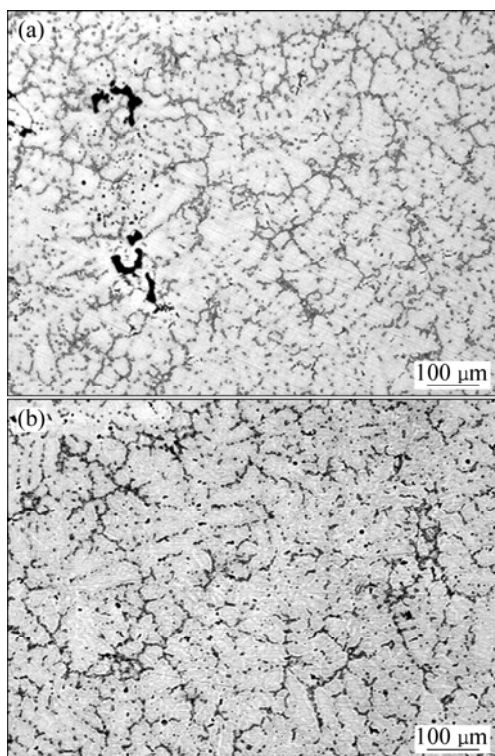


Fig.8 SEM images of sample purified by only gas bubbling (a) and combination of ceramic filter and gas bubbling (b)

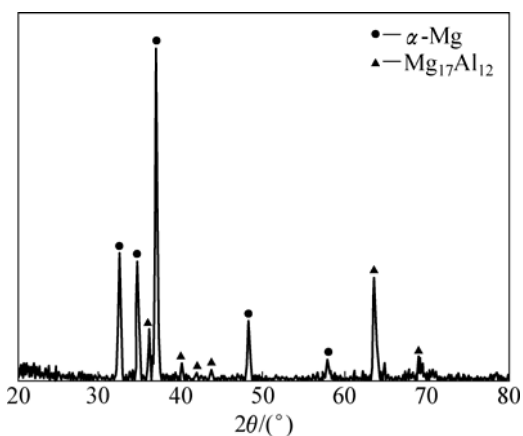


Fig.9 X-ray diffraction pattern of AZ91 alloy purified by gas bubbling

The fracture surfaces of the unrefined sample after tensile tests are shown in Fig.10. The images show a brittle fracture surface with large oxide clusters in as-cast samples. The fracture paths follow the inclusions and they are clearly exposed. The fracture surface of the sample after gas bubbling and filtration purification is shown in Fig.11. No inclusion is found on the fracture surface and the fracture is quasi-cleavage crack. Though the micro-morphology feature of the fracture seems to be river pattern of cleavage crack, the fracture pattern is not genuine cleavage fracture but belongs to transcrystalline fracture, for the fracture surface is mixed with small cleavage planes, steps, tear arrises and rivers. Compared Fig.10 with Fig.11, it can be concluded that

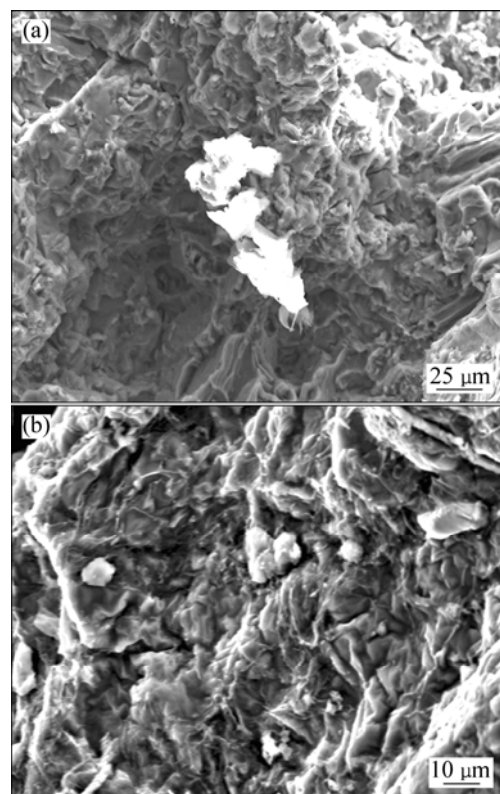


Fig.10 Fracture surfaces of unrefined sample

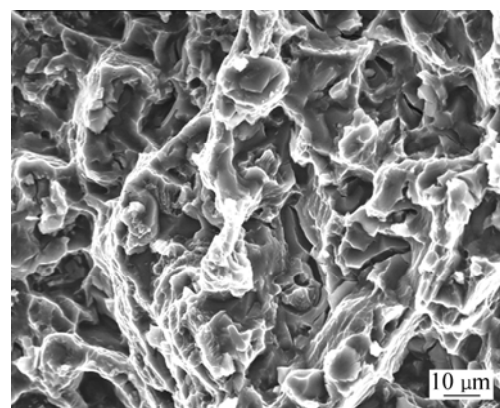


Fig.11 Fracture surface of sample after gas bubbling and filtration

filtration process has a certain effect on the fracture pattern of AZ91 alloy.

4 Discussion

4.1 Gas bubbling

Non-flux refining includes all refining processes where salt is not used, such as settling, floatation and filtration. Gas bubbling processes are usually used to remove the hydrogen and inclusions in the aluminum melt. Because the densities of the inclusions are often smaller than that of aluminum, these processes are very effective in purification of aluminum alloy melt. Recently, it has been claimed that gas purging of magnesium alloys can remove a lot of inclusions from the melt. Since magnesium is a very light metal, the densities of inclusions in the melt are often slightly higher than that of magnesium alloys, it might be expected that the heavier inclusions would settle to the bottom of the crucible. However, as discussed previously, many particles can float up. Probably, the explanation is that they are covered by gas layer. Perhaps water vapor and dissolved hydrogen play a role in creating the gas layer. A fact is that particles prefer gas to the magnesium melt: they are wetted by gas, which indicates that particles may be floated up by gas purging. Only inert gas can be employed since the presence of reactive gases such as chlorine or fluorine-containing gases would give salts. When gas is injected into the melt, the impurities come into contact with the bubbles by various effects such as inertia, interception, gravitation and diffusion. If the impurities are wetted by the bubbles not the melt, there is a high probability that the impurities remain trapped at the bubble-melt interface and are carried up to the dross.

The following is the analysis about the inclusion movement in the melts. To describe the movement of inclusions in the melt, it is assumed that the inclusions adhere to the spraying gas once they touch the gas and the gas around the inclusions. The stress condition of the single inclusion in the Mg melt is shown in Fig.12.

According to stress equilibrium relationship:

$$F_b + F_f = F_w$$

Then,

$$(V_{inclusion} \rho_{inclusion} + V_{gas} \rho_{gas})g = V \rho_{metal}g + \frac{1}{2} C_d \rho_{metal} A u^2 \tag{1}$$

that is,

$$(V_{inclusion} \rho_{inclusion} + V_{gas} \rho_{gas})g - V \rho_{metal}g = \frac{1}{2} C_d \rho_{metal} A u^2 \tag{2}$$

Take the spherical particle as a example, then,

$$V_{inclusion} = \frac{4}{3} \pi r_{inclusion}^3$$

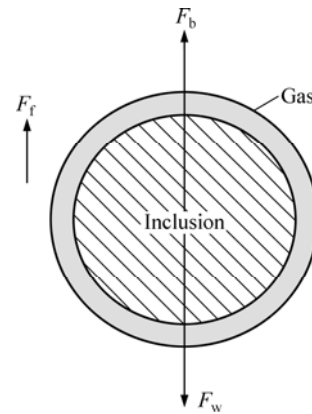


Fig.12 Schematic diagram of inclusion particle with gas covered (F_b Particle buoyant force; F_w Particle gravity force; F_f Viscosity resistance)

$$V = \frac{4}{3} \pi r^3$$

$$V_{gas} = V - V_{inclusion} \quad (r > r_{inclusion})$$

$$A = \pi r^2$$

$$C_d = \frac{24}{Re}$$

$$Re = \frac{2r u \rho_{metal}}{\eta_{metal}}$$

then,

$$u = \frac{2g}{9\eta_{metal}r} [r_{inclusion}^3 (\rho_{inclusion} - \rho_{gas}) + r^3 (\rho_{gas} - \rho_{metal})] \tag{3}$$

where u is the particle settling velocity; g is the gravity acceleration; η_{metal} is the viscosity coefficient; $r_{inclusion}$ is the inclusion particle radius; r is the radius of aggregate of inclusion absorbing gas; $\rho_{inclusion}$ is the inclusion density; ρ_{gas} is the gas density; ρ_{metal} is the metal density; $V_{inclusion}$ is the inclusion particle volume; V is the volume of aggregate of inclusion absorbing gas; V_{gas} is the gas particle volume; C_d is the drag coefficient; A is the projected area of a particle; Re is the Reynolds number.

During gas bubbling, after gas spraying into the Mg melt, the inclusion particles are wetted by gas, then r increases. In this case, according to Eq.(3), it can be inferred that with the increase of r , u decreases. If the gas flow rate is somewhat small, then the residual quantity of inclusions in the final castings maybe increases because of the too slow settling velocity. In this case, the mechanical properties of castings will decrease. However, if the spraying gas flow rate is large enough, r will become large enough. In this case, according to Eq.(3), for $\rho_{gas} - \rho_{metal}$ is negative, u might become negative when

r is large enough. This means that the aggregation of inclusions will not settle, but float to the melt surface. Besides, with large spraying gas flow rate, the gas has a large force to push the inclusions to the melt surface. The above two aspects help to decrease the residual inclusion content in the final castings and increase the mechanical properties of the alloys. This explains why the σ_b and σ_s of gas bubbling sample at small flow rate are lower than those of the sample from the fresh melt and the properties can be improved at high flow rate.

On the other hand, the solubility of hydrogen gas in both solid and liquid magnesium is well documented, and it is believed that hydrogen contributes to micro-porosity and micro-shrinkage in final castings[9–12]. Hydrogen can be potentially absorbed into molten magnesium from various sources including: hydrocarbon residues from various lubricants left on scrap, chemically bound water in hygroscopic fluxes, a humid atmosphere and /or excess combustion gases. The removal of hydrogen is necessary since the absorption of hydrogen gas into molten magnesium is very easy to happen. Spraying inert gas is a common technique utilized to degas aluminum and aluminum alloys. Fortunately, the same benefits are realized in magnesium alloys. Ref.[13] researched the effect of gas spraying on the hydrogen content of Mg melt. The results show that gas bubbling process can decrease the hydrogen content in the Mg melt to decrease the micro-porosity and micro-shrinkage. This also helps to improve the mechanical properties of the alloys.

4.2 Filtration

CFF is a kind of high efficient filtering medium for alloy melt[14–15]. In order to lower the content of detrimental particles prior to casting, filtration with CFF is common in casting of aluminum. It has also been applied to steels.

Fig.3(b) shows the morphology of a CFF used in this experiment. The skeleton of dense and tiny ceramic branches in the CFF forms a continuous three-dimensional structure. Its filtration mechanism is fairly complicated. At present, the dominant views related to the mechanism include the following three aspects. The first factor is filtering action. That is, inclusion particles are counterchecked by tiny holes in the filter so that the accumulation of inclusions even leads to the formation of inclusion cakes. Furthermore, the formed inclusion cakes help to hold the smaller inclusion particles in the melt. The second factor is the existence of many winding tiny tunnels in the filtration medium. Some tiny particles deposit at the corners of the passage due to the fluctuation of the fluid speed. The third factor is its excellent adsorption capability. This is because the huge surface of the skeleton, which is not

wetted by the metal melt, has strong adsorption for solid tiny inclusion which is not wetted by the melt. As a result of the synthetic effects of the above three factors, excellent filtration efficiency can be obtained. This kind of filter can remove the solid inclusion particles the diameter of which is less than 10–20 μm .

Molten metal filtration often puts two incompatible requirements on the industrial filter: 1) large volumes of metal should be filtered before the pressure drop over the filter becomes too large; 2) the filter should remove virtually all inclusions. Therefore, filtration is often a matter of compromise between filter life and metal cleanliness.

Generally, the filtration theory can be distinguished into two modes, i.e. depth filtration and cake filtration. In depth filtration, the inclusions are captured inside the filter, while in cake filtration the inclusions get stuck on other inclusions in front of the filter. In this work, because the fresh ingots are used, cake filtration hardly occurs, only depth filtration is discussed. In this case, inclusions much smaller than the filter pore size are removed deeply down in the filter.

The most important parameter in filtration process is filtration efficiency, E it can be expressed as

$$E = \frac{C_0 - C_{\text{out}}}{C_0} = 1 - \exp(-\eta\alpha_s\beta L) \quad (4)$$

where C_0 is the concentration of inclusions in the unfiltered metal; C_{out} is the concentration of inclusions in the filtered metal; η is the collision efficiency; α_s is the surface area per unit volume length; β is the ratio of the collector surface projected in the flow direction to the total collector surface area; L is the thickness of the filter.

An important example is a filter consisting of spherical collectors of diameter $2R$. The void fraction in the filter is denoted ε . Then, $\beta=1/4$ and

$$E = 1 - \exp\left[-\frac{3\eta L(1-\varepsilon)}{4R\varepsilon}\right] \quad (5)$$

For the direct interception mechanism it is found that the collision efficiency $\eta=3d/2R$, where d is the inclusion diameter. Then,

$$E = 1 - \exp\left[-\frac{9dL(1-\varepsilon)}{8R^2\varepsilon}\right] \quad (6)$$

According to Eq.(6), the filtration efficiency is an increasing function of inclusion size. For CFFs, the filtration efficiency increases as inclusion size increases and filter pore size decreases.

From Eq.(6), it can be also seen that filtration efficiency E increases with the increase of filter thickness L . C_{dep} denotes the concentration of particles deposited per unit filter length. The inclusion deposition function inside a filter then can be written as

$$C_{\text{dep}}(z)=C_0\eta\alpha_s\beta\exp(-\eta\alpha_s\beta z) \quad (7)$$

where z is the distance from a point inside the filter to the surface of the filter from which the melt floats into the filter and $0 < z < L$.

Eq.(7) predicts that when inclusions are assumed to be completely mixed in the transverse direction of the flow, the particle deposition decreases exponentially as a function of z .

This means that a CFF of certain thickness can effectively remove the inclusions in the melt. With further increase of filter thickness, the decrease content of inclusions is limited. The results in Fig.5(b) confirms this analysis, which show that σ_b and δ increase with the increase of filter thickness. The results may be due to the inclusions decrease in the alloy. Fig.9 also shows that the CFF of 15 mm in thickness can effectively improve σ_b and δ . When the thickness increases from 15 to 20 mm, σ_b and δ only improve from 187.9 MPa and 3.89% to 189.3 MPa and 4.02% by 0.7% and 3.3%, respectively.

The industrial filter should have large pores so that a relatively small metal head is needed to force metal into the entire filter. A filter with large depth filtration capability and good filtration efficiency should be employed. Therefore, it has large void fractions and a large internal surface. According to our experiments, filters with large ppi (more than 20 ppi) will choke the flow of metal and lead to low filter efficiency. It is concluded that 15–20 ppi is the optimal porosity size.

Based on the above research and analysis, it leads to a conclusion that both filtration and inert gas spraying techniques should be utilized together to remove inclusions and dissolved hydrogen gas from magnesium melt effectively.

5 Conclusions

1) Non-flux refining of magnesium is a practical method to improve σ_b and δ of AZ91 alloy. The large inclusion agglomeration can be dispersed and non-metallic inclusions can be removed to some extent by gas spraying process.

2) Ar spraying with high flow rate can remove non-metallic inclusions and improve the mechanical properties of the alloy. Ar spraying for 30 min at melt temperature of 740 °C helps to get best properties. The mechanical properties decrease with further increase of spraying time and temperature.

3) The CFF can effectively improve the σ_b and δ of AZ91 alloy, especially δ . Filtration is more effective for AZ91 scraps than for AZ91 fresh alloy. Both σ_b and δ increase with increasing ppi and the thickness of CFF. The CFFs of no more than 20 ppi are suitable for filtrating AZ91 alloy.

4) Both filtration and inert gas spraying techniques should be utilized together to improve the mechanical properties effectively, they do not change the microstructure of AZ91 alloy. Filtration has a certain effect on the fracture pattern of AZ91 alloy. The fracture surface of the sample after gas bubbling and filtration shows that no inclusions are found on the fracture surface and the fracture pattern is quasi-cleavage crack.

References

- [1] WU Yu-feng, DU Wen-bo, NIE Zuo-ren, CAO Lin-feng, ZUO Tie-yong. Thermodynamic calculation of intermetallic compounds in AZ91 alloy containing calcium [J]. Transactions of Nonferrous Metals Society of China, 2006, 16(2): 392–396.
- [2] WANG Wei, WU Guo-hua, WANG Qu-dong, HUANG Yu-guang, SUN Ming, DING Wen-jiang. Investigation of flux containing GdCl₃ on recycling Mg-Gd-Y-Zr scraps [J]. Transactions of Nonferrous Metals Society of China, 2008, 18(Special 1): s292–s298.
- [3] YANG Ming-bo, PAN Fu-sheng, CHENG Ren-ju, TANG Ai-tao. Effects of Al-10Sr master alloys on grain refinement of AZ31 magnesium alloy [J]. Transactions of Nonferrous Metals Society of China, 2008, 18(1): 52–58.
- [4] GAO Hong-tao, WU Guo-hua, DING Wen-jiang, ZHU Yan-ping. Purifying effects of new flux on magnesium alloy [J]. Transactions of Nonferrous Metals Society of China, 2004, 14(3): 530–536.
- [5] WU Guo-hua, ZHAI Chun-quan, ZENG Xiao-qin, ZHU Yan-ping, DING Wen-jiang. Study on purification technology of magnesium alloy wastes [J]. Transactions of Nonferrous Metals Society of China, 2003, 13(6): 1260–1264.
- [6] BELL S, DAVIS B, JAVAID A, ESSADIQI E. Final report on refining technologies of magnesium [R]. Ontario Canada: Davis Laboratories, 2006.
- [7] SHALEV G, MOSCOVITCH N, BRONFIN B, RUBINOVICH Z, AGHION E. Fluxless recycling of creep resistant die casting magnesium alloys MRI 153M & MRI 230D [C]// 12th Magnesium Automotive and End User Seminar. Aalen, Germany Dead Sea Magnesium Ltd, 2004: 1–10.
- [8] HOUSH S E, PETROVICH V. Magnesium refining: A fluxless alternative [J]. Society of Automotive Engineers, 1992: 1–7.
- [9] OVRELED E, ENGH T A, OYMO D. Hydrogen measurement in pure and alloyed magnesium [C]// Light Metals 1994. San Francisco, California, USA, 1994: 771–778.
- [10] HUANG Y C, WATANABE T, KOMATSU R. Hydrogen in magnesium and its alloys [C]// Proceedings of the 4th International Conference on Vacuum Metallurgy, Tokyo: Iron and Steel Institute of Japan, 1974: 173–176.
- [11] BAKKE P, LAURITZEN J L, ENGH T A, OYMO D. Hydrogen in magnesium absorption, removal and measurement [J]. Light Metals, 1991: 1015–1023.
- [12] TALBOT D E J. Effects of H in Al, Mg, Cu and their alloys [J]. International Metallurgical Reviews, 1975, 20(19): 166–184.
- [13] GALOVSKY U, KUHLEIN M. A new conti-process for the fluxless recycling of high purity magnesium [C]//Magnesium Technology 2001. New Orleans, USA, 2001: 49–53.
- [14] CAO Xin-jin. A new analysis of pressure filtration curves for liquid aluminum alloys [J]. Scripta Materialia, 2005, 52(9): 839–842.
- [15] RIGO O D, OTUBO J, C MOURA NETO, MEI P R. NiTi SMA production using ceramic filter during pouring the melt [J]. Journal of Materials Processing Technology, 2005, 162/163: 116–120.
- [16] BAKKE P, ENGH T A, BATHEN E, OYMO D, NORDMARK A. Magnesium filtration with ceramic foam filters and subsequent quantitative microscopy of the filters [J]. Materials and Manufacturing Processes, 1994, 9(1): 111–138.

(Edited by FANG Jing-hua)